CHINESE OPTICS LETTERS

Vol. 20, No. 7 | July 2022

Inverse design of 1D color splitter for high-efficiency color imaging

Jiahao Li (黎家豪)[1,†], Mengwei Cao (曹孟威)[1,2,†], Weili Liang (梁伟立)[1], Yilin Zhang (张屹林)[1], Zhenwei Xie (谢振威)[1*], and Xiaocong Yuan (袁小聪)[1]

[1] Nanophotonics Research Center, Shenzhen Key Laboratory of Micro-Scale Optical Information Technology & Institute of Microscale Optoelectronics, Shenzhen University, Shenzhen 518060, China

[2] Department of Physics, Harbin Institute of Technology, Harbin 150001, China

*Corresponding author: ayst3_1415926@sina.com

Received February 1, 2022 | Accepted April 14, 2022 | Posted Online April 29, 2022

We introduce a simple one-dimensional (1D) structure in the design of 1D color splitters (1D-CSs) with RGB unit cells for color imaging and propose a single-to-double-layer design in 1D-CSs. Based on inverse design metasurfaces, we demonstrate numerically a single-layer 1D-CS with a full-color efficiency of 46.2% and a double-layer 1D-CS with a full-color efficiency of 48.2%; both of them are significantly higher than that of traditional color filters. Moreover, we demonstrate a 1D-CS that has application value by evaluating the double-layer 1D-CS's performances in terms of incident angle sensitivity, polarization angle sensitivity, and assembly tolerance.

Keywords: color splitter; color imaging; inverse design; metasurfaces.
DOI: 10.3788/COL202220.073601

1. Introduction

Since color filters allow high selectivity of individual colors and simple image processing, using color filters to separate red (R), green (G), and blue (B) bands has always been a research hotspot in color imaging[1–3]. As the pixel sizes of color image sensors are becoming smaller and smaller to meet higher-resolution color imaging, the incoming average photon count per pixel is also becoming less and less[4,5]. This trend brings challenges to color filters for its inherent ∼2/3 light losses in each color pixel filter, whether in one-dimensional (1D) color filters such as RGB arrays with RGB unit cells or two-dimensional (2D) color filters such as Bayer filter arrays with RGB unit cells[6].

In the past decade, the color splitter (CS), having sub-wavelength structure and full-band transmission characteristics in visible light, was proposed to provide an alternative to the color filter and received a lot of attention from researchers[7,8]. In theory, the splitter can increase the photon collection per pixel up to three times, making it possible to achieve a higher optical efficiency than a traditional filter. However, due to the complexity in color splitting and diffracting, the design of the splitter with high efficiency, high resolution, and easy processing is always a thorny problem, even in the simplest 1D-CS with RGB unit cells. For example, the device's designs by introducing traditional nanostructures have difficulties in multiwavelength color splitting according to specific bands like R, G, and B wavelength bands and have a low average spectral efficiency in each pixel[9,10].

To date, metasurfaces[11–18] have been widely used to study various optical effects at the sub-wavelength scale and performed exceptional functions. NTT Device Technology Laboratories in Japan proposed a pixel-scale 1D-CS based on a dielectric metasurface that only has an average spectral efficiency of ∼40% in each pixel, limited by the design methods[19]. Then, Philip's team has successfully demonstrated an ultra-efficient (> 80%) 1D-CS by increasing the design freedom of the device, in which they combine 1D-CS with an inverse design based on adjoint optimization[20–23]. However, this 1D-CS is hard to fabricate and is compatible to current complementary metal-oxide-semiconductor (CMOS) processing technology due to its complicated 3D spatial structure. Recently, designed by an inverse design with a genetic algorithm (GA), a 1D-CS with an efficiency of ∼45% and with a 2D structure of a quick response (QR) code has been demonstrated[24], striking a balance between efficiency and processing. However, there are still many problems in this 1D-CS that need to be improved, such as increasing the splitter's efficiency, reducing the thickness and geometric complexity of the device to make it easier to process, reducing the crosstalk from different frequency bands, essentially instead of combining the splitter and filter to increase the cost, and speeding up the design process.

Here, we propose two 1D structure 1D-CSs based on TiO_2 metasurfaces and show a single-to-double-layer design to further improve the 1D color splitting efficiency of the 1D-CS in color imaging. The size of the 1D-CS unit cell is only 3 μm in width and 0.3 μm in thickness, and, because of its simple 1D structure, its length can be arbitrary, it requires less computing resources than other 1D-CSs with 2D or 3D structures, and it is easier to process theoretically. We show in simulations that the single-layer 1D-CS has an average efficiency of up to 46.2% across the entire visible spectrum (380–780 nm), and the average efficiency of the double-layer 1D-CS is up to 48.2%; both of them are significantly higher than that of traditional color filters (~33.3%, theoretical maximum value without considering other optical loss). The total design time including the single-layer and the double-layer 1D-CS is within a week. Moreover, we evaluate the double-layer 1D-CS's performances in terms of incident angle sensitivity, polarization angle sensitivity, and assembly tolerance, demonstrating a 1D-CS with application value.

2. Methods

Device geometry in 2D and 3D is widely adopted to design 1D-CSs, especially in the methods of inverse design, which certainly increases the design freedom of the device by exploring more unknown structures[20,24]. But, they also slow down the design process, caused by a large number of optimization data. What is more, there is no need to use such complex structures to design 1D-CSs because their light wave is only deflected or diffracted in the 1D direction. In contrast, device geometry with 1D refractive index distribution is excellent enough for 1D-CSs according to the principles of optical diffraction, which to our knowledge has not been investigated previously. Therefore, inspired by the design of 1D grating couplers[25,26], we create a 1D structure consisting of a high refractive index material and a low refractive index material to design our 1D-CSs, as depicted in S1 in Fig. 1(b). We take titanium dioxide (TiO_2) as this high refractive index material (n decreases from 2.399 to 2.098 in the wavelength range of 380–780 nm, according to Ref. [27]) for its high transmittance in the full-color band and mature processing technology[28–30], and it would be better to take air as the low refractive index material ($n \approx 1$) for the same reasons. The whole RGB unit cell shown in Fig. 1(a) reflects the fundamental color splitting schematic and compactness of our 1D-CS unit cell. The full-color band (380–780 nm) transmitting through the unit cell with a width of 3 μm will be focused on three different pixels with a width of 1 μm according to its wavelength. For increasing the design freedom of the 1D-CS unit cell and considering the current fabrication capability at the same time, this 1D-CS unit cell consists of 60 bars, and each bar that can be TiO_2 or air randomly has a cross-section dimension of 50 nm × 300 nm, where 300 nm is the thickness of the 1D-CS. This thickness can provide about half-wavelength (or phase π) modulation under the visible band when we change the refractive index of the bar. To better reflect the color characteristics of the band, the R, G, and B bands here are defined as 580–780 nm, 480–580 nm, and 380–480 nm, respectively.

Undoubtedly, the 1D structure above is simple enough that any current inverse design methods for multidimensional space optimization are adequately suited for the optimization of this 1D-CS to obtain good performance. Here, the simulated annealing (SA) algorithm is skillfully applied to this 1D-CS, which is our previous experience in designing an orbital angular momentum (OAM) emitter[31,32]. The SA inspired by the principle of solid annealing is one of the global optimization algorithms, and it utilizes a cooling schedule (initial temperature, cooling rate, chain length, and termination condition) to control the optimization process. In implementation, the 60 bars in the 1D-CS unit cell will be replaced by a set of binary strings consisting of 0 and 1. During the iteration, better generation for the device structure is selected according to random probability

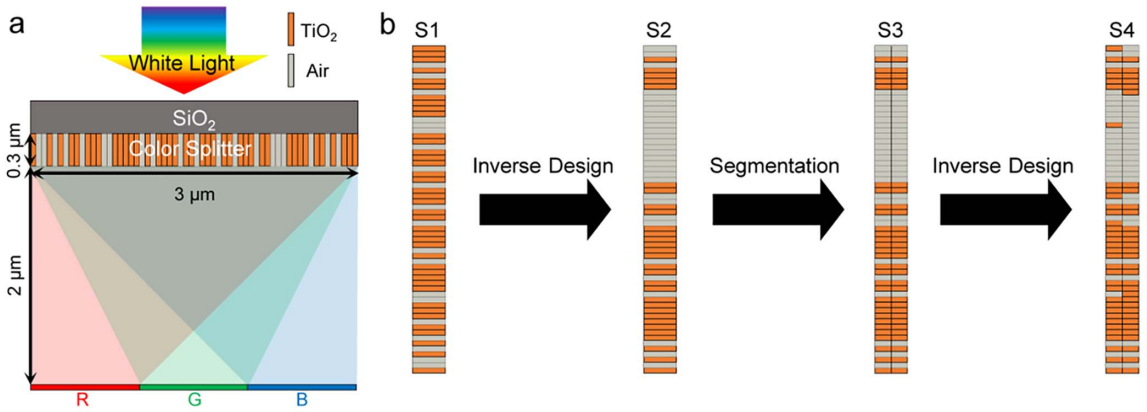

Fig. 1. Compact 1D-CS designed by the inverse design. (a) Schematic diagram of 1D-CS. The spectral range of incident light is 380–780 nm, and the diffraction distance is 2 μm behind the device. There are three target imaging areas (pixels) R, G, and B distributed in the 1D direction. (b) Schematic illustrating the design of a double-layer splitter created from a single-layer one. Structures S1, S2, S3, and S4 represent the initial structure of the single-layer splitter, the final structure of the single-layer splitter, the initial structure of the double-layer splitter, and the final structure of the double-layer splitter, respectively. All devices' structures in the figure above are cross sections.

based on Metropolis criterion that is affected by real-time temperature. We set the number of iterations at each temperature as 500 and the cooling equation as $T_n = 0.95nT_0$, where the cooling rate is 0.95, $T_0 = 0.02$ is the initial temperature, and T_n is the temperature for the nth iteration. By inverse design with SA, a final structure of the single-layer splitter with 1D color splitting performance will be obtained from a 1D random structure, as shown in the process of S1 to S2 in Fig. 1(b). To achieve more precise phase modulation, we need to implement the optimization search in a wider solution space. Inspired by the segmented hierarchical evolutionary algorithm[32], we segment the single-layer 1D-CS into a double-layer 1D-CS without changing its total thickness, as shown in the process of S2 to S3 in Fig. 1(b). Then, taking S3 as a new initial structure, a final structure of the double-layer splitter with better 1D color splitting performance will be obtained by adopting the similar method above, as shown in the process of S3 to S4 in Fig. 1(b). The entire process in Fig. 1(b) can be finished within a week by finite-difference time-domain (FDTD) and a single server with the Dell T7920 model and NVIDIA Quadro P2000 graphics cards.

3. Results

The color responses of the designed 1D-CSs are shown in Fig. 2. An outstanding color splitting performance is achieved by the designed single-layer 1D-CS with structure S2, demonstrated by its simulated spectra [Fig. 2(a)] and by its simulated field distributions in the cross section under three bands [Figs. 2(c)–2(e)]. By calculation, the average efficiency of this device is 46.2% across the entire visible spectrum (380–780 nm), and that of each color band is 45.2%, 45.4%, and 48.0%, respectively, where the efficiency is defined as the ratio between the flux of energy for corresponding color pixel and the flux of energy of incident light for the 1D-CS unit cell, showing the spectrum focusing ability of the splitter. In contrast, the designed double-layer 1D-CS with structure S4 has a slight improvement in focusing performance by its simulated spectra and field distributions, as shown in Figs. 2(b) and 2(f)–2(h), and it has an average efficiency of 48.2% across three bands (48.4%, 47.1%, and 49.2% for each band, respectively). Compared to schemes that combine splitters and filters to reduce crosstalk, both of our 1D-CSs exhibit a low crosstalk, making it possible to be filter-free. In terms of commercialization costs, the single-layer 1D-CS is excellent enough because it is also the simplest structure at present, which means that it has the simplest preparation process under such compactness.

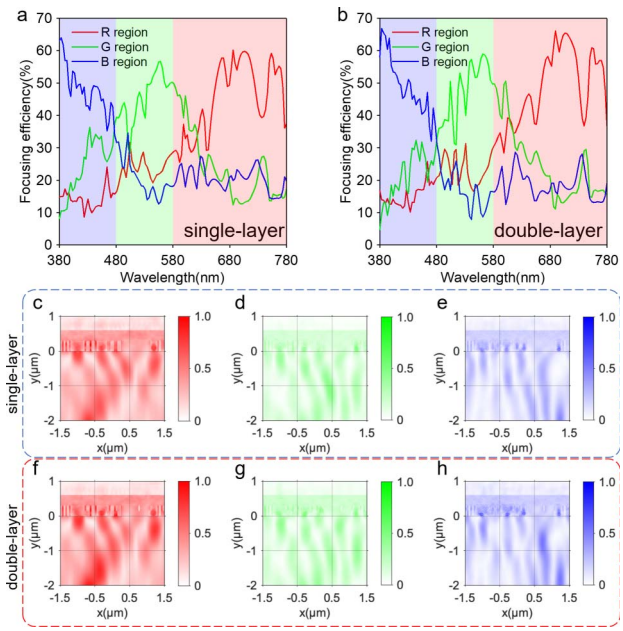

Fig. 2. Simulated splitting characteristics of the designed splitter, calculated from FDTD Solutions. (a) Visible light focusing efficiency of the single-layer splitter at different target color regions (pixel). (b) Visible light focusing efficiency of the double-layer splitter at different target color regions. (c), (d), (e) Field plots at the transmission plane of the single-layer device operating under (c) R (580–780 nm), (d) G (480–580 nm), and (e) B (380–480 nm) light. (f), (g), (h) Field plots at the transmission plane of the double-layer device operating under (f) R (580–780 nm), (g) G (480–580 nm), and (h) B (380–480 nm) light.

The angle sensitivity is another important factor to evaluate the 1D-CS's performances, including incident angle sensitivity and polarization angle sensitivity. Except for some special application scenarios like polarization cameras, in most cases, the improvement of average efficiency across the entire visible band at a cost of large incident angle sensitivity and polarization angle sensitivity is not expected. Taking the double-layer 1D-CS as an example, we analyze its sensitivity characteristics in the incident angle and polarization angle shown in Fig. 3, calculated from the software named FDTD Solutions. Here, we define the average efficiency above 40% across three bands (RGB) as acceptable efficiency. This 1D-CS has an acceptable incident angle range of −4.7° to 3.3° [Fig. 3(a)] along the splitting direction (x) that is the most sensitive direction, and we believe it could have a better range than that if we consider all directions. The simulated field distributions in the cross section under the incident angles of −4.7° and 3.3° along the splitting direction are shown in Figs. 3(c)–3(e) and 3(f)–3(h), respectively. Compared with the field plots in Figs. 2(f)–2(h), these field distributions maintain similar profiles but slightly shift in position, resulting in a decline in splitting functionality. Moreover, this 1D-CS exhibits a considerable polarization independence, as shown in Fig. 3(b), where the average efficiency across three bands is higher than 40% for most of the polarization angle. We select two representative polarization angles of 45° and 90° to demonstrate their splitting characteristics through their field distributions, as shown in Figs. 3(i)–3(k) and 3(l)–3(n), respectively. Compared with the field plots in Figs. 2(f)–2(h), these field distributions still work well in the R band, slightly bad in the G band, and obviously bad in the B band, and that of the polarization angle of 90° is worse than that of the polarization angle of 45°, corresponding to the effect shown in Fig. 3(b). For different color bands, it will have distinctly different responses, both in incident and polarization angle sensitivity, resulting in uneven color splitting, which is a common problem that exists in all 1D

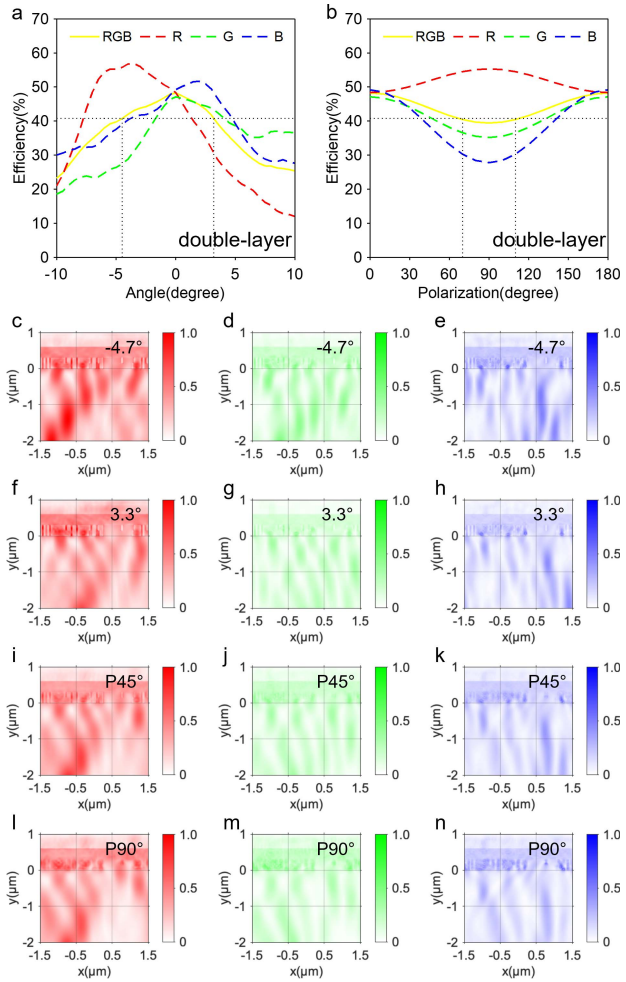

Fig. 3. Simulated sensitivity characteristics of the designed double-layer splitter, calculated from FDTD Solutions. (a) Incident angle sensitivity along the splitting direction (*x*). Yellow curve corresponds to the average efficiency of three bands (RGB). The R, G, and B curves correspond to the average efficiency of R (580–780 nm), G (480–580 nm), and B (380–480 nm) light, respectively. (b) Polarization angle sensitivity. Yellow curve corresponds to the average efficiency of the three bands (RGB). R, G, and B curves correspond to the average efficiency of R (580–780 nm), G (480–580 nm), and B (380–480 nm) light, respectively. (c)–(h) Field plots at the transmission plane under incident angles of (c)–(e) −4.7° and (f)–(g) 3.3° along the splitting direction (*x*), operating under (c), (f) R (580–780 nm), (d), (g) G (480–580 nm), and (e), (h) B (380–480 nm) light. (i)–(n) Field plots at the transmission plane under polarization angles of (i)–(k) 45° and (l)–(n) 90°, operating under (i), (l) R (580–780 nm), (j), (m) G (480–580 nm), and (k), (n) B (380–480 nm) light.

and 2D-CSs, due to the different optical paths resulting from its wavelength.

To further evaluate the application value of our 1D-CS, we explore the assembly tolerance of our double-layer 1D-CS in simulation, as shown in Figs. 4(a) and 4(b). Still taking 40% as an acceptable efficiency, we show a 1D-CS with an excellent lateral tolerance of [−0.28 μm, 0.55 μm], which means that our device can be misaligned with pixels along the color splitting direction and still maintains a good performance within large

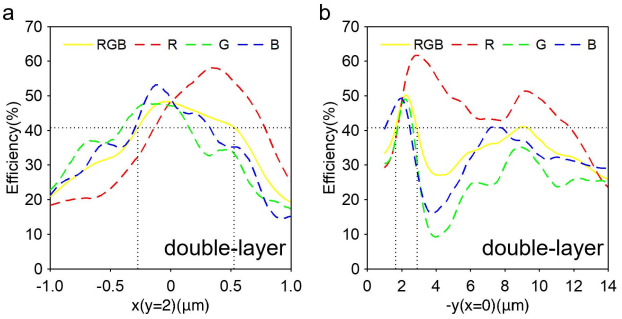

Fig. 4. Simulated assembly tolerance of the designed double-layer splitter, calculated from FDTD Solutions. (a) Lateral tolerance. Device moves along the color splitting direction (*x*). (b) Longitudinal tolerance. Device moves along the diffraction direction (*y*). Yellow curve corresponds to the average efficiency of the three bands (RGB). The R, G, and B curves correspond to the average efficiency of R (580–780 nm), G (480–580 nm), and B (380–480 nm) light, respectively.

error. In longitudinal (diffraction direction) tolerance, our 1D-CS exhibits an excellent tolerance of [−2.9 μm, −1.6 μm] as well, and, different from the angle sensitivity above, the three color bands show a similar behavior in longitudinal tolerance. Besides, the Talbot effect can be found in the position of 9.05 μm below our 1D-CS, and the average efficiency is up to 41.1% across the three bands in this position, which is likely to be applied in future research.

4. Conclusion

The 1D structure 1D-CSs including the single-layer and double-layer are proposed for high-efficiency color imaging, and a single-to-double-layer design is presented by introducing the inverse design two times. From the perspective of device cost, the single-layer 1D-CS has great potential commercial value in high-efficiency, high-resolution color imaging for its simpler structure than the current 1D-CS, more compact size, and high efficiency of 46.2%. Although the performance of the double-layer 1D-CS is only slightly improved over that of the single-layer one, we still believe that the single-to-double-layer design method is promising not only in CSs but also in other photonic devices.

Acknowledgement

This work was supported by the Guangdong Major Project of Basic and Applied Basic Research (No. 2020B0301030009), National Natural Science Foundation of China (Nos. 61935013, 61975133, and 11947017), Natural Science Foundation of Guangdong Province (No. 2020A1515011185), Science and Technology Innovation Commission of Shenzhen, Shenzhen Peacock Plan (Nos. KQJSCX20170727100838364, KQTD20170330110444030, ZDSYS201703031605029, and JCYJ20200109114018750), and Shenzhen University (No. 2019075).

†These authors contributed equally to this work.

References

1. J. Liu, K. Feng, Y. Wang, Q. Li, N. Chen, and Y. Bu, "High-color-purity, high-brightness and angle-insensitive red structural color," Chin. Opt. Lett. **20**, 021601 (2022).
2. B. Zeng, Y. Gao, and F. J. Bartoli, "Ultrathin nanostructured metals for highly transmissive plasmonic subtractive color filters," Sci. Rep. **3**, 2840 (2013).
3. Y. D. Shah, P. W. R. Connolly, J. P. Grant, D. Hao, C. Accarino, X. Ren, M. Kenney, V. Annese, K. G. Rew, Z. M. Greener, Y. Altmann, D. Faccio, G. S. Buller, and D. R. S. Cumming, "Ultralow-light-level color image reconstruction using high-efficiency plasmonic metasurface mosaic filters," Optica **7**, 632 (2020).
4. S. G. Wuu, C. C. Wang, B. C. Hseih, Y. L. Tu, C. H. Tseng, T. H. Hsu, R. S. Hsiao, S. Takahashi, R. J. Lin, C. S. Tsai, Y. P. Chao, K. Y. Chou, P. S. Chou, H. Y. Tu, F. L. Hsueh, and L. Tran, "A leading-edge 0.9 μm pixel CMOS image sensor technology with backside illumination: future challenges for pixel scaling," in *International Electron Devices Meeting* (2010), p. 14.1.1.
5. Q. Chen, X. Hu, L. Wen, Y. Yu, and D. R. Cumming, "Nanophotonic image sensors," Small **12**, 4922 (2016).
6. B. E. Bayer, "Color imaging array," U.S. patent 3,971,065-A (July 20, 1976).
7. P. Camayd-Muñoz, C. Ballew, G. Roberts, and A. Faraon, "Multifunctional volumetric meta-optics for color and polarization image sensors," Optica **7**, 280 (2020).
8. E. Johlin, "Nanophotonic color splitters for high-efficiency imaging," iScience **24**, 102268 (2021).
9. T. Shegai, S. Chen, V. D. Miljkovic, G. Zengin, P. Johansson, and M. Kall, "A bimetallic nanoantenna for directional colour routing," Nat. Commun. **2**, 481 (2011).
10. S. Nishiwaki, T. Nakamura, M. Hiramoto, T. Fujii, and M.-a. Suzuki, "Efficient colour splitters for high-pixel-density image sensors," Nat. Photon. **7**, 240 (2013).
11. N. Yu, P. Genevet, M. A. Kats, F. Aieta, J. P. Tetienne, F. Capasso, and Z. Gaburro, "Light propagation with phase discontinuities: generalized laws of reflection and refraction," Science **334**, 333 (2011).
12. N. Yu and F. Capasso, "Flat optics with designer metasurfaces," Nat. Mater. **13**, 139 (2014).
13. S. Wang, P. C. Wu, V. C. Su, Y. C. Lai, M. K. Chen, H. Y. Kuo, B. H. Chen, Y. H. Chen, T. T. Huang, J. H. Wang, R. M. Lin, C. H. Kuan, T. Li, Z. Wang, S. Zhu, and D. P. Tsai, "A broadband achromatic metalens in the visible," Nat. Nanotechnol. **13**, 227 (2018).
14. M. Parry, A. Mazzanti, A. Poddubny, G. D. Valle, D. N. Neshev, and A. A. Sukhorukov, "Enhanced generation of nondegenerate photon pairs in nonlinear metasurfaces," Adv. Photonics **3**, 055001 (2021).
15. A. Overvig and A. Alù, "Wavefront-selective Fano resonant metasurfaces," Adv. Photonics **3**, 026002 (2021).
16. X. Wang, J. Xin, Q. Ren, H. Cai, J. Han, C. Tian, P. Zhang, L. Jiang, Z. Lan, J. You, and W. E. I. Sha, "Plasmon hybridization induced by quasi bound state in the continuum of graphene metasurfaces oriented for high-accuracy polarization-insensitive two-dimensional sensors," Chin. Opt. Lett. **20**, 042201 (2022).
17. Z. Yue, J. Li, C. Zheng, J. Li, M. Chen, X. Hao, H. Xu, Q. Wang, Y. Zhang, and J. Yao, "Manipulation of polarization conversion and multiplexing via all-silicon phase-modulated metasurfaces," Chin. Opt. Lett. **20**, 043601 (2022).
18. S. Cai, W. Hu, Y. Liu, J. Ning, S. Feng, C. Jin, L. Huang, and X. Li, "Optical fiber hydrogen sensor using metasurfaces composed of palladium," Chin. Opt. Lett. **20**, 053601 (2022).
19. M. Miyata, M. Nakajima, and T. Hashimoto, "High-sensitivity color imaging using pixel-scale color splitters based on dielectric metasurfaces," ACS Photonics **6**, 1442 (2019).
20. P. Camayd-Munoz, G. Roberts, M. Debbas, C. Ballew, and A. Faraon, "Inverse-designed spectrum splitters for color imaging," in *Conference on Lasers and Electro-Optics* (2019), paper AM4K.3.
21. S. Molesky, Z. Lin, A. Y. Piggott, W. Jin, J. Vucković, and A. W. Rodriguez, "Inverse design in nanophotonics," Nat. Photon. **12**, 659 (2018).
22. A. Y. Piggott, J. Lu, K. G. Lagoudakis, J. Petykiewicz, T. M. Babinec, and J. Vučković, "Inverse design and demonstration of a compact and broadband on-chip wavelength demultiplexer," Nat. Photon. **9**, 374 (2015).
23. B. Shen, P. Wang, R. Polson, and R. Menon, "An integrated-nanophotonics polarization beamsplitter with 2.4×2.4 μm^2 footprint," Nat. Photon. **9**, 378 (2015).
24. M. J. Chen, L. Wen, D. H. Pan, D. R. S. Cumming, X. G. Yang, and Q. Chen, "Full-color nanorouter for high-resolution imaging," Nanoscale **13**, 13024 (2021).
25. A. Y. Piggott, J. Lu, T. M. Babinec, K. G. Lagoudakis, J. Petykiewicz, and J. Vuckovic, "Inverse design and implementation of a wavelength demultiplexing grating coupler," Sci. Rep. **4**, 7210 (2014).
26. C. Xie, X. Zou, F. Zou, and Y. Zhang, "High-performance ultra-compact polarization splitter-rotators based on dual-etching and tapered asymmetrical directional coupler," Chin. Opt. Lett. **19**, 121301 (2021).
27. https://refractiveindex.info/?shelf=main&book=TiO2&page=Devore-o.
28. S. Sun, Z. Zhou, C. Zhang, Y. Gao, Z. Duan, S. Xiao, and Q. Song, "All-dielectric full-color printing with TiO_2 metasurfaces," ACS Nano **11**, 4445 (2017).
29. Y. K. Wu, W. H. Yang, Y. B. Fan, Q. H. Song, and S. M. Xiao, "TiO_2 metasurfaces: from visible planar photonics to photochemistry," Sci. Adv. **5**, eaax0939 (2019).
30. D. Wen, J. J. Cadusch, J. Meng, and K. B. Crozier, "Light field on a chip: metasurface-based multicolor holograms," Adv. Photon. **3**, 024001 (2021).
31. Z. Xie, T. Lei, F. Li, H. Qiu, Z. Zhang, H. Wang, C. Min, L. Du, Z. Li, and X. Yuan, "Ultra-broadband on-chip twisted light emitter for optical communications," Light Sci. Appl. **7**, 18001 (2018).
32. Z. Jin, S. Mei, S. Chen, Y. Li, C. Zhang, Y. He, X. Yu, C. Yu, J. K. W. Yang, B. Luk'yanchuk, S. Xiao, and C. W. Qiu, "Complex inverse design of meta-optics by segmented hierarchical evolutionary algorithm," ACS Nano **13**, 821 (2019).